Environmental Science & Technology

pubs.acs.org/est

Article

Insights into the Biogeochemical Cycling of Cobalt: Precipitation and Transformation of Cobalt Sulfide Nanoparticles under Low-Temperature Aqueous Conditions

Muammar Mansor,* Elizabeth Cantando, Yi Wang, Jose A. Hernandez-Viezcas, Jorge L. Gardea-Torresdey, Michael F. Hochella, Jr., and Jie Xu*

Cite This: https://dx.doi.org/10.1021/acs.est.0c01363

Read Online

ABSTRACT: Cobalt sulfide precipitates, key phases in the natural biogeochemistry of cobalt and in relevant remediation and resource recovery processes, are poorly defined under low-temperature aqueous conditions. Here, we systematically studied Co (Fe) sulfides precipitated and aged in environmentally relevant solutions, defined by different combinations of pH, initial cobalt to iron ratios ($[Co]_{aq}/[Fe]_{aq}$), with/without S^0, and the presence/absence of sulfate-reducing bacteria. The initial abiogenic precipitates were composed exclusively of amorphous Co sulfide nanoparticles ($CoS{\cdot}xH_2O$) that were stable in anoxic solution for 2 months, with estimated log K^* values 1−5 orders of magnitude higher than that previously reported for Co sulfides. The addition of S^0, in combination with acidic pH and elevated temperature (60 °C), resulted in recrystallization of the amorphous precipitates into nanocrystalline jaipurite (hexagonal CoS) within 1 month. In the presence of $Fe(II)_{aq}$, the abiogenic precipitates were composed of more crystalline Co sulfides and/or Co-rich mackinawite, the exact phase being dependent on the $[Co]_{aq}/[Fe]_{aq}$ value. The biogenic precipitates displayed higher crystallinity for Co sulfides (up to the formation of nanocrystalline cobalt pentlandite, Co_9S_8) and lower crystallinity for Co-rich mackinawite, suggestive of mineral-specific bacterial interaction. The revealed precipitation and transformation pathways of Co (Fe) sulfides in this study allows for a better constraint of Co biogeochemistry in various natural and engineered environments.

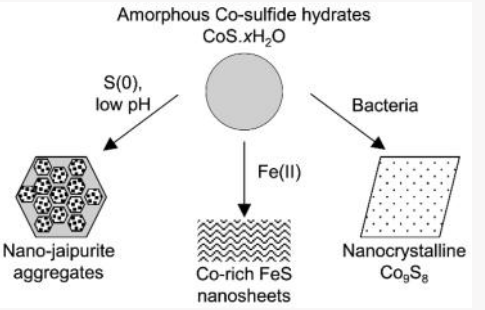

INTRODUCTION

Cobalt (Co) is a biologically and environmentally important trace metal that is an integral component of cobalamin (e.g., vitamin B12), which is essential for various key biological functions in all domains of life.[1−5] At high concentrations, cobalt can cause detrimental effects to microbial, plant, animal, and human metabolisms.[6−8] The increasing anthropogenic release of Co into the environment has been a growing concern for the United States Environmental Protection Agency[9] and the Department of Energy,[10] especially in areas close to mining sites, coal power plants, cobalt alloy factories, highways, and nuclear reactors.[8] At the same time, recovering Co from industrial and mining byproducts is highly desirable from an economic perspective due to the scarcity of Co-bearing ores and the ever-increasing uses of Co in modern technology.[11] Thus, there is significant interest in effectively immobilizing and concentrating Co in a stable form, especially from aquatic systems, either for long-term remediation or for resource recovery and subsequent reuse.

One of the most promising methods for sequestering Co and other heavy metals in anoxic−suboxic environments involves the addition of sulfide (from abiotic sources or from sulfate-reducing bacteria), which readily reacts with metal cations to form relatively insoluble metal sulfide precipitates.[12−14] Due to the extremely low solubility of metal sulfides under anoxic−suboxic conditions, aqueous metal cations can be sequestered with high efficiency in the form of nanosized particles.[15,16] This process could have naturally occurred at oceanic scales in the sulfidic oceans on the early Earth and thus may have played an important part in constraining the bioavailability of Co and the evolution of ancient life.[17,18] In all of these cases, information on the stability and reactivity of Co sulfides is crucial to determine the cycling patterns and fate of Co. The stability and reactivity of metal sulfide nanoparticles are known to be strongly affected by their formation pathways and resultant physicochemical properties (e.g., size, crystallinity, phase, shape),[19−23] all of which are poorly characterized for Co sulfides.

To fill this vital knowledge gap, we have undertaken a study to characterize the initial precipitates and transformation

Received: March 4, 2020
Revised: March 28, 2020
Accepted: April 3, 2020
Published: April 3, 2020

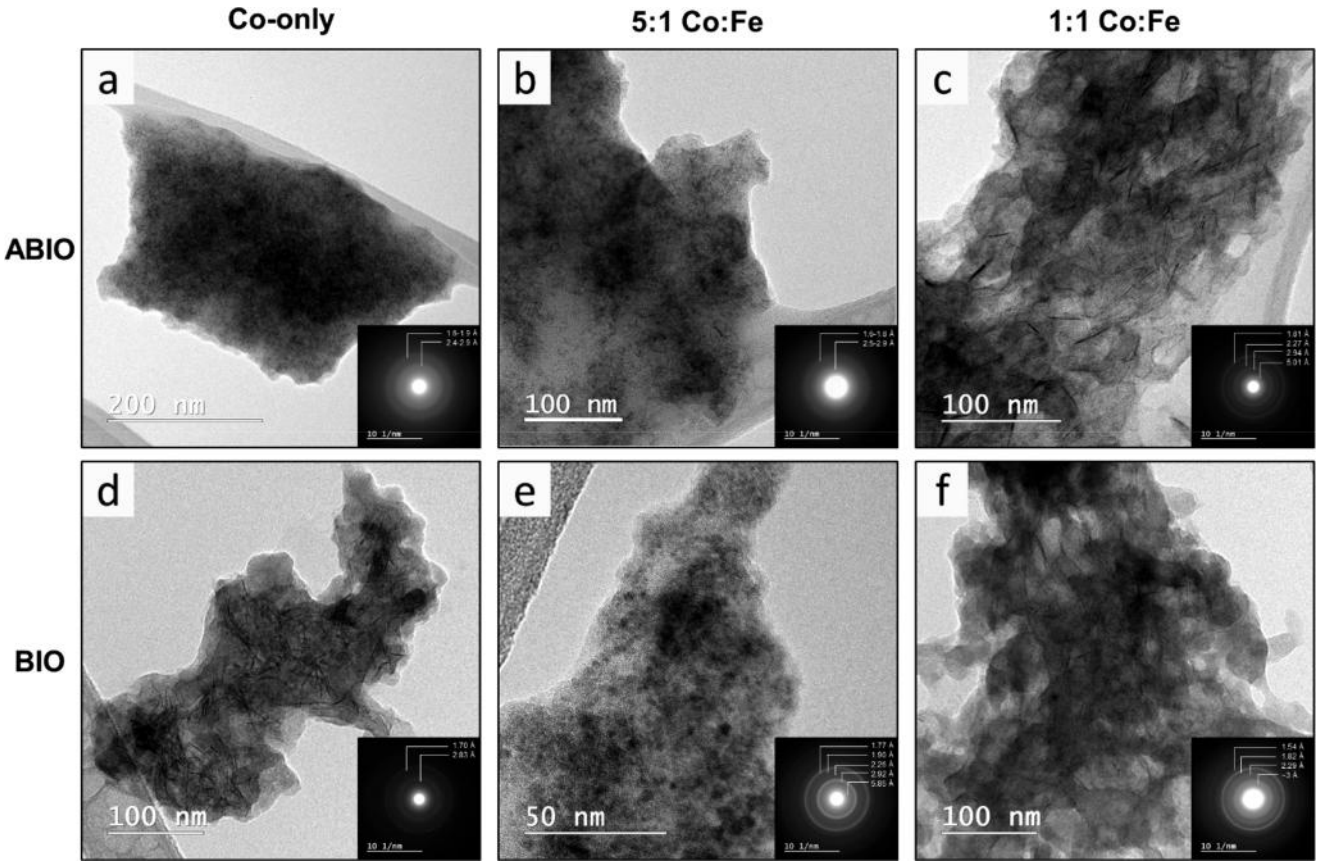

Figure 1. Low-magnification microscopy images of abiogenic (top) and biogenic (bottom) Co−Fe−sulfide precipitates at different initial $[Co]_{aq}/[Fe]_{aq}$ in the near-neutral pH experiments, focusing on the bulk structure of the aggregates. Insets display representative SADPs. (a−c) Aggregates of the abiogenic precipitates are generally amorphous to poorly crystalline. Higher crystallinity (more surface textures and sharper diffraction rings) is observed with increasing initial $[Fe]_{aq}$ content (from left to right). (d−f) The biogenic precipitates share similar structures with the abiogenic precipitates, albeit with differences in crystallinity (more crystalline and sharper diffraction rings for "Co-only" and 5/1 ratio; less crystalline and more diffuse diffraction rings for 1/1 ratio). In (e), darker spots corresponding to the presence of nanocrystalline cobalt pentlandite are visible. Images in (a)−(d) are from 5 day old samples, while images in (e) and (f) are from 30 day old samples.

products of Co sulfides precipitated under low-temperature aqueous conditions, through a combination of electron microscopy based methods, X-ray diffraction (XRD), and inductively coupled plasma atomic emission spectroscopy (ICP-OES). Precipitation and aging conducted in various environmentally relevant solutions—defined by different combinations of pH, initial Co to iron(II) ratios ($[Co]_{aq}/[Fe]_{aq}$), with/without elemental sulfur (S^0), and the presence/absence of sulfate-reducing bacteria (SRB)—revealed a range of nanosized products, from amorphous Co sulfides to nanocrystalline jaipurite (CoS), cobalt pentlandite (Co_9S_8), and Co-rich mackinawite ((Co,Fe)S). The results from our study will aid in refining predictive models aimed at exploring the mobility and fate of Co in the environment.

MATERIALS AND METHODS

All syntheses were performed under anoxic conditions following previously established methods by our group.[24,25] Abiogenic Co sulfides were precipitated via slow titration or immediate pouring of 50 mL of $Na_2S{\cdot}9H_2O$ into 50 mL of modified metal toxicity medium (MTM) amended with aqueous Co(II) and/or Fe(II) (see Table S1 for the medium composition). The total amount of added sulfide was kept constant at a concentration of 7.5 mM in the mixed solution (without considering precipitation), while the total concentration of metals ranged from 0.5 to 5 mM. The initial $[Co]_{aq}/[Fe]_{aq}$ ratio was varied among "Co-only", 5/1, 1/1, 1/2, and 1/5. Abiotic experiments were performed under two pH conditions, acidic (pH 2.9, rising to pH 3.6 after sulfide addition) and near-neutral (pH 7.2, rising to 8.6 after sulfide addition), to cover the wide range of pH in natural and engineered environments. Elemental sulfur was also amended to some of the abiotic experiments (concentration equivalent of 6.3 mM in the mixed solution) to examine the effect of additional oxidant and sulfur source on phase transformations.[26−28] Abiotic experiments were carried out mostly at room temperature (~25 °C), with a few at elevated temperature (60 °C, inside an incubator), for up to 60 days. Additionally, biogenic metal sulfides were precipitated in metal-amended MTM inoculated at 1% (v/v) with an exponential-phase cell culture medium of *Desulfovibrio vulgaris*. The initial total metal concentrations in the biological experiments were kept constant at 0.5 mM, while the biogenic sulfide concentration reached a maximum of 15 mM over a period of 90 days of incubation at 30 °C. A schematic of the complete experimental design is shown in Figure S1.

The precipitates were collected via centrifugation and/or filtration through 0.2 μm mixed cellulose ester (MCE) filter papers. X-ray diffraction patterns of the bulk material—dried as thin films on glass slides inside an anaerobic chamber—were

https://dx.doi.org/10.1021/acs.est.0c01363
Environ. Sci. Technol. XXXX, XXX, XXX−XXX

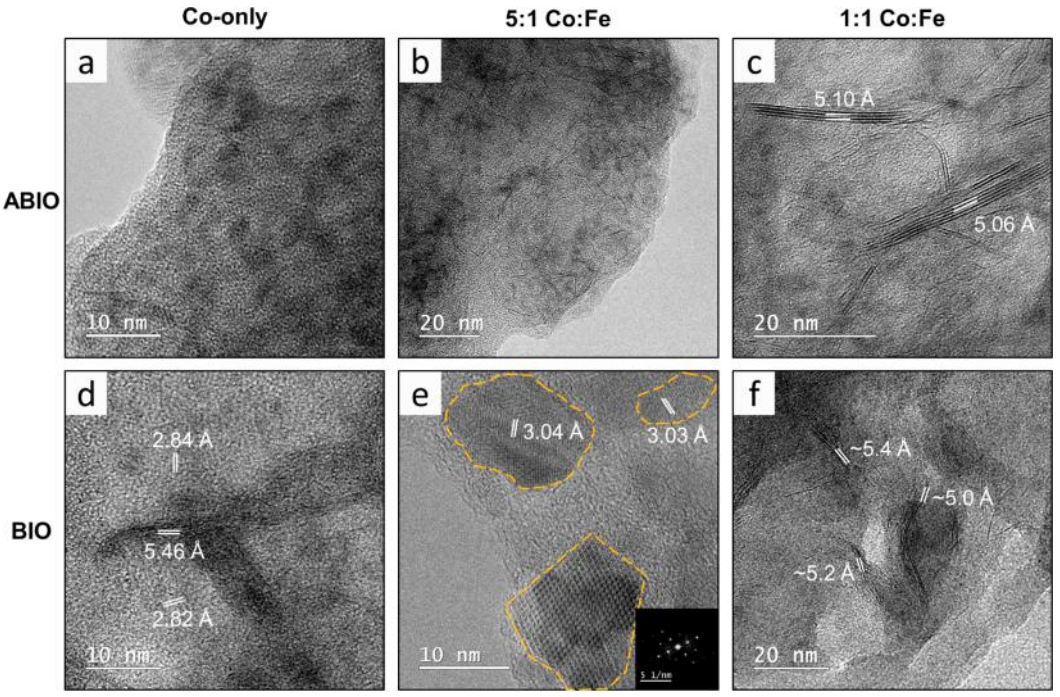

Figure 2. High-magnification microscopy images of abiogenic (top) and biogenic (bottom) Co−Fe−sulfide precipitates at different initial $[Co]_{aq}/[Fe]_{aq}$ in the near-neutral pH experiments, focusing on the internal structure of the nanoparticle aggregates. (a) Amorphous structure of abiogenic Co sulfides. (b) At a 5/1 ratio, fibrous textures are evident on the surface of the aggregates. (c) At a 1/1 ratio, crystalline acicular textures are evident on the surface of the aggregates. (d) Biogenic Co sulfides containing nanodomains on the surfaces of the aggregates. (e) At a 5/1 ratio, 10−20 nm domains (top, outlined in yellow) and particles of $(Co,Fe)_9S_8$ (bottom, outlined in yellow) are evident within larger-sized biogenic aggregates. The inset corresponds to the diffraction pattern (obtained from fast Fourier transform) of the crystalline Co_9S_8 nanoparticle adjacent to it. (f) At a 1/1 ratio, fibrous textures are evident on the surface of the biogenic aggregates. Images in (a)−(d) are from 5 day old samples, while images in (e) and (f) are from 30 day old samples.

obtained using a Rigaku Miniflex II with a 2θ range of 10−60° and a total scan time of 105 min/sample. For transmission electron microscopy (TEM) analysis, the collected precipitates were resuspended in anoxic water and shipped in sealed glass vials to the NanoEarth National Center at Virginia Tech, where the suspended materials were mounted onto TEM grids for analysis on a JEM-2100 instrument coupled with an energy dispersive X-ray spectrometer (EDS). The biogenic samples were pretreated with lysozyme and proteinase K to remove residual organics that might interfere with high-resolution imaging. Control experiments using abiogenic samples indicated that enzymatic treatment did not cause changes to the metal sulfides, consistent with previous studies.[20] Extra steps were taken to minimize oxidation and to identify oxidation products (if any) during these analyses, as detailed in the Discussion in the Supporting Information. Any samples displaying oxidation features were discarded from interpretation.

For ICP-OES analyses, the collected precipitates were redispersed and washed in N_2-degassed ethanol and then centrifuged at 2000*g* for 5 min to remove the supernatant. This washing step was repeated three times altogether. The precipitates were dried for 2 days inside an anaerobic chamber and then digested through the following sequence: (a) overnight digestion of 20−40 mg of the solids in 3.5 mL of concentrated HNO_3 at 25 °C in screw-capped containers (the strongly oxidizing HNO_3 likely promoted oxidation of H_2S to sulfate, thus minimizing the loss of sulfur as volatiles in subsequent steps), (b) heating at 115 °C for 45 min with the cap opened, (c) mixing with 2 mL of 30% H_2O_2 after cooldown, followed by another heating at 115 °C for 20 min with the cap opened, and (d) dilution with 3% HNO_3 prior to ICP-OES analysis. Ethanol-washed and dried precipitates were also examined using Fourier transform infrared spectroscopy (FTIR, in attenuated total reflectance mode) and thermogravimetric analysis (TGA) for the presence of structural water. Each TGA analysis utilized about 2 mg of solids that were sequentially heated to 600 °C at a rate of 5 °C/min under a nitrogen flow, and the final data were corrected for empty-pan baseline. Several standards including powdered FeS (product #343161-1G, Sigma-Aldrich), powdered CoS (product #13114, Alfa Aesar), and crushed pyrite grains (<150 μm, from Spain), were analyzed alongside the samples. These solid standards, while differing significantly from freshly precipitated nanoparticles especially in terms of size and crystallinity, are suitable materials to test the accuracy of ICP-OES analysis and for comparative FTIR and TGA analyses on water-free metal sulfides.

Aqueous Co and sulfide concentrations were measured via ICP-OES and the methylene blue assay (Hach Co., Colorado), respectively. Solutions were sampled via needles and syringes through a tightly affixed rubber stopper, filtered through 200 nm pore size cellulose acetate membranes, and then either acidified to 3% HNO_3 (for Co) or fixed with 20% $ZnCl_2$ and stored at −20 °C (for sulfide) prior to analysis. A subset of the samples was also passed through a centrifugal filter with a 3 KDa NMWL cutoff (equivalent to filters with ∼1 nm pore size; product #UFC500396, Millipore Sigma) while being centrifuged at 14000*g* for 30 min to test for the contribution of nanosized particles to the aqueous concentrations.

https://dx.doi.org/10.1021/acs.est.0c01363
Environ. Sci. Technol. XXXX, XXX, XXX−XXX

Table 1. List of Known Minerals in the Co−Fe−Sulfide System, along with Associated Crystal Chemistry and *d* Spacings (in Å)

	mineral					
	amorphous Co sulfide[a]	cobalt pentlandite	jaipurite[b]	linnaeite	cattierite	mackinawite
cryst structure	amorphous to poorly crystalline	cubic	hexagonal	cubic	cubic	tetragonal
chem composition	$CoS_{1.00-1.38}{\cdot}xH_2O$	$(Co,Fe)_9S_8$	CoS	Co_3S_4	CoS_2	(Co,Fe)S
S/Me ratio	1.38−1.00	0.89	1.00	1.33	2.00	1.00
d spacing (*hkl*)[c]	*5.5*	**5.73 (111)**				
						5.03 (001)
				3.33 (220)		
					3.20 (111)	
		2.99 (311)				2.97 (101)
			2.92 (100)			
		2.86 (222)		2.84 (311)		
					2.77 (200)	
	2.4−2.9; *2.8*		**2.54 (101)**			
					2.48 (210)	
				2.35 (400)		2.31 (111)
		2.28 (331)			2.26 (211)	
		1.91 (511)	1.93 (102)		1.96 (220)	
						1.84 (200)
				1.81 (511)		1.81 (112)
		1.75 (440)				
						1.73 (201)
	1.6−1.9; *1.7*		1.68 (110)	1.67 (440)	1.67 (311)	
					1.60 (222)	
					1.54 (302)	
					1.48 (321)	
		1.24 (800)	1.27 (202)	1.23 (731)	1.27 (331)	
					1.13 (422)	

[a]Chemical composition and sulfur to metal (S/Me) ratios are compiled on the basis of data from this study and those of Loussot et al.[29,30] and Sun et al.[39] This material is also known as *cobalt oxysulfide* in earlier studies. The *d* spacings for this material are derived from only this study; ranges of *d* spacings are listed for those associated with the poorly crystalline abiogenic Co sulfides, while single values (italicized) are listed for *d* spacings associated with the more crystalline biogenic Co sulfides. [b]Classified by the International Mineralogical Association as a "questionable" mineral phase, referring to a mineral that is recognized as valid on the basis of historical observations but with some level of doubt and in need of re-examination. [c]*d* spacing data for crystalline phases compiled from the American Mineralogist Crystal Structure Database (http://rruff.geo.arizona.edu/AMS/amcsd.php; accessed on April 28, 2019) and filtered to exclude minor reflection planes (<10 relative intensity in XRD). Boldface values indicate mineral-specific *d* spacings, defined as those values that are separated by >±0.05 Å (typical measurement error of SADP and high-resolution imaging of lattice fringes) from other reflection planes.

RESULTS AND DISCUSSION

Initial Precipitates of Abiogenic Co Sulfides. The addition of sulfide to a Co-containing solution resulted in the formation of black precipitates either immediately or within a few hours depending on the rate of sulfide addition. Regardless of the pH (acidic or near-neutral), the rate of sulfide addition, and the initial sulfide to metal ratios, the precipitates collected within 60 days of incubation at room temperature were largely XRD-amorphous (Figure S2), indicative of the lack of long-range order. A broad XRD signal centered at approximately 15−17° 2θ (5.2−5.9 Å) was tentatively distinguishable relative to the background. Electron microscopy analyses indicated that the precipitates were composed of amorphous aggregates, with no clear lattice fringes at high resolutions (Figure 1a and 2a). The selected area electron diffraction patterns (SADPs) for these aggregates revealed two diffuse diffraction rings, with *d* spacings in the ranges of 2.4−2.9 Å (centered at ∼2.6 Å) and 1.6−1.9 Å (centered at ∼1.7 Å), respectively. No diffraction ring corresponding to the *d* spacing of 5.2−5.9 Å was identified, although it was possible that this signal was obscured by the bright transmitted beam spot. This set of *d* spacings is not diagnostic of any known crystalline phases of Co sulfides (Table 1).

The sulfur to cobalt (S/Co) ratios of the initial precipitates were determined via ICP-OES to be 1.22 (mean of two synthesis batches; Table S2) and via EDS to be 0.99 ± 0.52 (n = 3 nanoscale aggregates). The two values agreed with one another within error. The large standard deviation associated with the EDS data may reflect actual compositional heterogeneity of the samples at the nanoscale, although the accuracy of this technique can be skewed by the inherent analytical error of EDS[29] and the presence of sulfur or metal species that adsorbed strongly to sulfide nanoparticles.[30,31] The values determined in this study were largely consistent with previously reported ratios of 1.03−1.38 for XRD-amorphous Co sulfides obtained by Loussot et al.[32,33] Loussot et al. also observed the co-occurrence of $Co(OH)_2$ via XRD and TEM in some of their samples, which could have skewed their S/Co ratios to values lower than the actual ones. Combining our data set with that of Loussot et al. suggests a relatively wide range of S/Co ratios for early-stage precipitates of Co sulfides, extending from near-stoichiometric to excess S over Co.

The poorly crystalline nature and probable nonstoichiometry of early-stage Co sulfides led us to consider if these Co sulfides may have incorporated structural water to help stabilize their crystal structure, similar to the case for

https://dx.doi.org/10.1021/acs.est.0c01363
Environ. Sci. Technol. XXXX, XXX, XXX−XXX

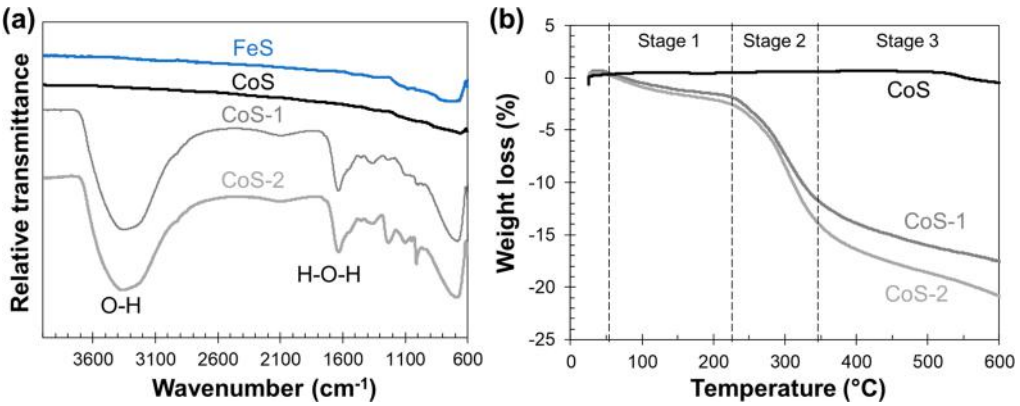

Figure 3. (a) FTIR patterns of crystalline FeS and CoS standards and two samples of abiogenic Co sulfides from different synthesis batches (CoS-1 and CoS-2; 5 days old). Bands centered at 1631 and 3300 cm^{-1} are attributable to water. Other bands at <1200 cm^{-1} are not easily assigned to a specific bond and likely originate from a combination of sulfide, cobalt, and oxygen stretching bands.[38,72] (b) TGA data (under N_2 flow) of crystalline CoS and abiogenic Co sulfides. Three stages of weight loss—differing in slope—are evident, as separated by vertical dashed lines.

nonstoichiometric nickel sulfide nanoparticles.[31,34] Interestingly, FTIR analysis did suggest the presence of water associated with the early-stage Co sulfides, on the basis of the broad bands centered at 1631 and 3300 cm^{-1}, respectively (Figure 3a). These water bands were absent in crystalline CoS (jaipurite−cobalt pentlandite mixture) and FeS (pyrrhotite) standards that were washed and dried in ways identical with those of the Co sulfide samples, thereby strongly suggesting that these bands were from structural water rather than adsorbed residual ethanol or water. Additionally, TGA analysis under a nitrogen flow showed that crystalline CoS remained stable (±2 wt %) upon heating up to 600 °C. This contrasted with the behavior of the precipitated Co sulfides, which experienced a weight loss of about 20% in three distinct stages over the same heating range (Figure 3b). The weight loss likely continued above 600 °C, although we did not test beyond that temperature. We interpreted the small weight loss during stage 1 to be due to the release of adsorbed water and/or ethanol, while the more significant and latter stages of weight loss (above ∼200 °C) were attributed to a protracted loss of structural water from differing atomic environments, similar to those observed for nickel sulfide nanoparticles.[31,34] Part of the weight loss may also be explained by a phase transition to crystalline Co sulfides, although previous studies noted that this process only occurs above 400 °C.[35,36] Overall, both FTIR and TGA analyses provided support for the presence of structural water associated with early-stage Co sulfides.

The results of our study were consistent with previous findings: mixing of aqueous Co and a sulfide source at low temperatures overwhelmingly produced XRD-amorphous precipitates.[32,33,37−40] Analyses via X-ray absorption spectroscopy suggested that Co is bonded to both sulfur and oxygen.[32,33,39,40] Loussot et al. termed this initial precipitate as "cobalt oxysulfide" and suggested a composition close to CoS(OH), although deviations from this ideal composition were observed to occur as a function of pH (tested up to pH 14 in that study), the initial sulfide to metal ratios, and the possible presence of trace amounts of $Co(OH)_2$.

On the basis of the available compilation, we therefore suggest that precipitation at room temperature will form XRD-amorphous abiogenic Co sulfides over a pH range of 3−14, with a composition of $CoS_{1.00-1.38}{\cdot}xH_2O$. The x symbol here represents the potential for varying amounts of associated water. At the nanoscale, these precipitates are associated with diffuse diffraction rings in the ranges of 2.4−2.9 and 1.6−1.9 Å, respectively. Aging in solution for 60 days at room temperature revealed a slight increase in crystallinity due to the detection of nanodomains (≲5 nm) of different morphology within the particle aggregates, although the derived SADPs remained indistinguishable relative to the early-stage precipitates (Figure S3). This precipitate was therefore stable in anoxic solution for at least 2 months despite its poor crystallinity.

Solubility of Abiogenic Co Sulfide Nanoparticles. We measured the aqueous Co concentration ($[Co]_{aq}$) in the experiments to constrain the solubility of early-stage Co sulfides. In the near-neutral pH experiments (pH 7−8), $[Co]_{aq}$ values after precipitation were consistently below the detection limit (∼10 μM) of ICP-OES. In comparison, the $[Co]_{aq}$ values in the acidic experiments (pH 2.9−3.6) were measurable and averaged 683 ± 71 μM after precipitation (Figure S4). This value was largely constant up to 180 days after precipitation. The measured $[Co]_{aq}$ in the <200 and <1 nm fractions agreed within 3% with one another, indicating a limited contribution of nanosized particles to the aqueous concentration data set. Concurrently, the sulfide concentrations averaged 3.81 ± 0.51 mM over the same period (Figure S4). The lower than expected values for sulfide concentrations (i.e., the initial value was ∼7.5 mM) likely indicated a combined loss via precipitation and rapid volatilization during sulfide addition into an acidic solution prior to capping of the containers. Sulfide concentrations remained largely constant afterward with the ending of precipitation and the tight capping of the experimental containers.

Assuming equilibrium condition was achieved within several days after initial precipitation, a 1/1 Co to sulfur stoichiometry, and the reaction

$$CoS{\cdot}xH_2O + 2H^+ \rightarrow Co^{2+} + H_2S_{aq} + xH_2O \quad (1)$$

we can determine the solubility product (log K^*) for amorphous Co sulfides at acidic pH (pH 3.6)

$$K^* = [H_2S_{aq}][Co^{2+}]/[H^+]^2 \quad (2)$$

using the CrunchFlow software package[41] with an updated database that considers several different species of Co(II) in solution. Further details are provided in the Supporting Information (SI Discussion and Tables S3 and S4). When the uncertainties in the speciation constants for aqueous Co−S

https://dx.doi.org/10.1021/acs.est.0c01363
Environ. Sci. Technol. XXXX, XXX, XXX−XXX

species and the experimentally determined concentrations of $[Co]_{aq}$ and sulfide at equilibrium are taken into account, the log K^* value for amorphous Co sulfides was constrained to be in the range of 0.9−1.4 (mean of 1.15 ± 0.25; Figure S5). This value is about 1−5 orders of magnitude higher than values reported for jaipurite (hexagonal CoS; log $K^* = -2.3$)[42] and unspecified phases of CoS listed in common thermodynamic databases (log $K^* = -0.37$ to −4.07; Table S4). Geochemical modeling using these databases would have significantly underestimated the amount of dissolved Co available in solution. Our study therefore reveals a previously unknown error in modeling efforts of Co biogeochemistry and highlights the necessity of further constraining the phase- and structure-specific solubility of Co sulfide nanoparticles for accurate predictive applications.

Transformation of Abiogenic Co Sulfides in the Presence of S^0 at Acidic pH. Cobalt is a redox-active element belonging in the transition-metal (Me) group. It is located between iron (Fe) and nickel (Ni) in the periodic table, and these elements share common oxidation states of +2 and +3 in the environment. Under sulfidic conditions, the initial precipitates of Fe and Ni undergo transformation from nanosized precursors to larger and better-defined crystals with the general formula of MeS (hexagonal structure), Me_3S_4, and/or MeS_2. The Co−S system contains equivalent phases in the form of jaipurite (hexagonal CoS), linnaeite (Co_3S_4), and cattierite (CoS_2) (Table 1). These phases have not been previously reported from precipitation at low temperature. The transformation reactions for Fe and Ni sulfides are typically accelerated in the presence of S^0, acidic pH, and/or higher temperatures.[25,28,43,44] We therefore attempted similar approaches to induce the transformation of early-stage Co sulfides to more crystalline phases.

In the presence of S^0, the bulk precipitates showed no XRD peaks corresponding to crystalline Co sulfides after 1 month of incubation at 60 °C, in both the acidic and near-neutral pH experiments (Figure S6). The precipitates from the 60 °C acidic experiments were analyzed further at the nanoscale using TEM. The 7 day old precipitates displayed characteristics similar to aggregates of Co sulfide nanoparticles, suggesting similarities in the initial precipitates irrespective of pH and the presence of S^0. After 30 days, however, nanoplates 60−170 nm in size and of high electron density were observable in addition to the amorphous aggregates (Figure S7). Closer observations revealed that each "nanoplate" was actually an aggregate of randomly oriented smaller nanoparticles, likely in the process of recrystallizing into a single crystal. This interpretation of the nanoplates' evolving crystal structure was supported by the corresponding SADPs, which displayed a set of diffraction rings, rather than distinct diffraction points expected from a single crystal. The associated d spacings of 2.87, 2.56, 1.94, and 1.64 Å are consistent with those of jaipurite (Table 1). To our knowledge, this is the first reported instance of jaipurite formation under relatively low temperature aqueous conditions. Furthermore, the evidence suggests that the growth was mediated in part by aggregation and attachments of smaller nanoparticles, consistent with other metal sulfides.[24,25,45]

Abiogenic Co−Fe−Sulfides at near-Neutral pH. The experiments on the Co-only systems have provided key information regarding the crystal structure and transformation of Co sulfide precipitates under anoxic aqueous conditions. These monometal experiments, however, did not reflect the complexity of the environments where two or more metals often exist alongside Co. Iron especially is a common metal in the environment, and Fe sulfides such as mackinawite (FeS) and pyrite (FeS_2) are known to incorporate significant amounts of Co into their crystal structures.[46−49] To better constrain the role of $Fe(II)_{aq}$ and Fe sulfides in Co sequestration, we performed a series of experiments at initial $[Co]_{aq}/[Fe]_{aq}$ molar ratios of 5/1, 1/1, 1/2 and 1/5, respectively, at near-neutral pH. The chosen ratios mimicked the diversity of natural environments, in which the $[Co]_{aq}/[Fe]_{aq}$ ratios can range from fairly high (up to 450) in some Co-rich streams affected by mining activities[50−52] to relatively low (down to 0.001) in other polluted sites[53−56] and pristine water bodies such as oceans and rivers.[57,58]

Our experimental results indicated that the crystallinities of the precipitates generally increased with increasing Fe(II) content, transitioning from XRD-amorphous at $[Co]_{aq}/[Fe]_{aq} \geq 1/1$ to XRD-detectable mackinawite at $[Co]_{aq}/[Fe]_{aq} \leq 1/2$ (Figure S2). The precipitates at $[Co]_{aq}/[Fe]_{aq}$= 5/1 and 1/1 were further characterized using TEM. At $[Co]_{aq}/[Fe]_{aq}$ = 5/1, the 5 day old precipitates were similar to the amorphous Co sulfide nanoparticles formed in Co-only systems, showing no lattice fringes at high resolution and only diffuse diffraction rings associated with d spacings of 1.6−1.8 and 2.5−2.9 Å, respectively (Figure 1b). Closer observations revealed additional features in the form of fibrous textures within the aggregates (Figure 2b). The fibrous textures were associated with d spacings of ∼5.5−6 Å, comparable to those associated with the tentative XRD shoulders at 2θ of 15−17° as described earlier (Figure S2). We therefore interpreted the abiogenic $[Co]_{aq}/[Fe]_{aq}$ = 5/1 precipitates to be a slightly more crystalline version of the precipitates observed in the Co-only experiments.

At $[Co]_{aq}/[Fe]_{aq}$ = 1/1, the precipitates formed within 5−60 days of incubation displayed higher crystallinity in comparison to the previous samples at higher $[Co]_{aq}/[Fe]_{aq}$. Specifically, the fibrous textures were replaced with crystalline acicular textures with d spacings of 5.0−5.1 Å (Figures 1c and 2c). The corresponding SADPs for the overall samples displayed clear diffraction rings with d spacings of 5.01, 2.94, 2.27, and 1.81 Å that were attributable to mackinawite, within an intrinsic analytical error of ±0.05 Å (Table 1). The Co/Fe ratios were determined to be 0.84 ± 0.07 (n = 3) via EDS and 0.85 ± 0.03 (n = 3) via ICP-OES, which were identical within error to the initial ratio of 0.82 (n = 1) for the initial solution (Table S2). Elemental maps obtained through EDS showed that Co and Fe were homogeneously distributed within the aggregates (Figure S8), indicating that the precipitate was most likely Co-rich mackinawite ($Fe_{1-y}Co_yS$), with $y \approx 0.45$. Although natural mackinawite is known to contain no more than 16.5 wt % of Co (y = 0.25),[48,49] a previous experimental study determined that the maximum value of y for Ni-substituted mackinawite is 0.56, and this study predicted a similar substitution limit of Co into mackinawite.[42] It is therefore possible that the value of y for Co-rich mackinawite can be as high as 0.45 as we estimated on the basis of the combined EDS and ICP-OES analyses. In fact, the Co−S and Fe−S bond chemistries are actually more similar to one another than to that of Ni−S (Table S5). Hence, it is within expectation that Co and Fe can readily substitute with one another within sulfide minerals. Overall, our experiments demonstrate that precipitation in the presence of Fe(II) significantly affects the crystallinity and the identity of the Co-bearing phases.

https://dx.doi.org/10.1021/acs.est.0c01363
Environ. Sci. Technol. XXXX, XXX, XXX−XXX

Biogenic Co−Fe−Sulfides at Near-Neutral pH. The last factor we have tested in this series of experiments is the effect of the presence of SRB on the physicochemical characteristics of the Co (Fe) sulfide precipitates. Sulfate-reducing bacteria are known to be the primary source of sulfide in low-temperature anoxic zones across the Earth's near-surface environments.[59] In addition to producing sulfide, the presence of microbial cells and their extracellular polymers have an influence on the size, phase, morphology, and aggregation state of metal sulfide precipitates, in addition to affecting the metal sulfide's aging and transformation processes.[20,60−63] In our biological experiments, biogenic precipitates were observed within 1−3 days following the inoculation of *D. vulgaris* into the amended medium. The slight variation in the timing of the initial precipitates is possibly due to inhibitory effects of $Co(II)_{aq}$ on the microbial growth. The pH remained relatively constant at 7.2 throughout the 90 day experiments. Similar to the case for abiogenic precipitates, the biogenic precipitates were largely XRD-amorphous at $[Co]_{aq}/[Fe]_{aq} \geq 1/1$, transitioning to XRD-detectable mackinawite at $[Co]_{aq}/[Fe]_{aq} \leq 1/2$ (Figure S2). Electron microscopy analyses, however, revealed nanoscale differences in the biogenic versus abiogenic precipitates under all of the tested conditions.

In the Co-only experiments, the biogenic precipitates collected after 5−90 days of incubation displayed sheetlike aggregate structures, with sharp diffraction rings associated with *d* spacings of 2.83 and 1.70 Å (Figure 1d). High-resolution TEM analyses revealed the presence of ∼10 nm crystalline domains with *d* spacings of around 2.8 Å and fibrous textures with *d* spacings of around 5.5 Å (Figure 2d). The S/Co ratios determined through EDS averaged 1.10 ± 0.18 (n = 6). These characteristics were comparable to those of abiogenic Co sulfides but with noticeably enhanced crystallinity, consistent with the results of previous studies. For example, Blessing et al. precipitated Co sulfides at near-neutral pH in the presence of *D. vulgaris* and concluded that the biogenic precipitates were structurally analogous to abiogenic Co sulfides on the basis of X-ray absorption spectroscopy.[13] Additionally, Krumholz et al. precipitated Co sulfides at pH 5.5−7.8 in pure cultures of SRB for up to 40 days. They determined that the precipitates were near-stoichiometric CoS through mass balance of the aqueous species.[14] Our analyses corroborated these earlier findings and also revealed a clear increase in crystallinity—indicated by sharper diffraction rings and the presence of fibrous textures—of the Co sulfides when precipitation occurred in the presence of SRB.

At $[Co]_{aq}/[Fe]_{aq}$ = 5/1, the biogenic precipitates formed after 6−30 days of incubation were composed of aggregates with associated nanodomains or nanoparticles about 5−20 nm in size (Figure 1e). The SADPs derived from the 6 day old precipitates were similar to those of the biogenic Co-only nanoparticles, displaying two diffraction rings with *d* spacings of around 2.8 and 1.7 Å. With aging, however, there was a clear increase in crystallinity. High-resolution TEM analyses of the 30 day old precipitates revealed the presence of nanodomains within the sheetlike structure, with *d* spacings corresponding to the (311) and (222) planes of cobalt pentlandite. Occasionally, highly crystalline 10−20 nm particles of cobalt pentlandite were evident (Figure 2e). The SADPs derived from these regions displayed a collection of five diffraction rings with corresponding *d* spacings of 5.85, 2.92, 2.26, 1.90, and 1.77 Å, respectively, consistent with the major reflection planes of cobalt pentlandite (Table 1). These findings were consistent with those of previous work, which reported the formation of nanocrystalline cobalt pentlandite particles in 7 month old enrichment cultures of SRB at initial $[Co]_{aq}/[Fe]_{aq}$ ratios ∼20/1.[64]

At $[Co]_{aq}/[Fe]_{aq}$ = 1/1, the biogenic precipitates formed after 30 days of incubation adopted a sheetlike morphology (Figure 1f). Crystalline nanoparticles of cobalt pentlandite were not observed at this $[Co]_{aq}/[Fe]_{aq}$ ratio. The derived SADPs revealed diffraction rings with a set of *d* spacings attributable to mackinawite. The diffraction rings of the biogenic precipitates were more diffuse in comparison to those of the abiogenic precipitates (sampled at day 5 and day 60), indicative of lower crystallinity. In support of this finding, high-resolution TEM analyses indicated the presence of fibrous textures on the surface of the biogenic precipitates (Figure 2f), in comparison to the more crystalline acicular textures observed for abiogenic mackinawite precipitated at the same $[Co]_{aq}/[Fe]_{aq}$ ratio (Figure 2c).

Overall, our results indicated that the presence of SRB can either increase (for Co-only and 5/1 ratio) or decrease the crystallinity (for 1/1 ratio) of Co-bearing phases relative to their abiogenic counterparts. This bidirectional trend was also observed in previous studies, whereby the presence of SRB tended to increase the crystallinity of most metal sulfides,[20,24,25,60,64−68] but not for all (i.e., copper sulfides).[24,61] Since we used the same SRB species throughout our study—thus eliminating variations in major types of organic metabolites—we interpreted these bidirectional effects mainly as a function of the surface properties of the metal sulfide themselves, which then affect the nature of the SRB−metal sulfide interactions and the subsequent recrystallization process. We hypothesize that in Co-only or high $[Co]_{aq}/[Fe]_{aq}$ systems dominated by Co sulfides, the presence of bacterial metabolites may have promoted recrystallization through reorganization and assembly of the amorphous nanoparticles (as previously demonstrated for zinc sulfides[20]). In contrast, in the lower $[Co]_{aq}/[Fe]_{aq}$ systems that were dominated by Co-rich mackinawite, the organic coating may have acted as a barrier that slowed down recrystallization (via nanoparticle assembly and/or partial oxidation in solution; multiple mechanisms can increase mackinawite's crystallinity[45,69−71]). Validation of this hypothesis relies on elucidating the nature of the SRB−metal sulfide interaction, which is nontrivial given the complex assemblages of organic molecules and crystal surface planes available. We note that previous studies reported increased crystallinities of trace-metal-free mackinawite in the presence of SRB,[24,60] indicating that metal substitutions may also modify the nature of the SRB−metal sulfide interactions. The development of an overarching theory for SRB−metal sulfide interaction, the properties of the resultant metal sulfides, and the specific mechanisms will be invaluable to the continued development of this field, especially for applications in biogeochemistry and bioengineering.

Environmental Implications. Cobalt is a bioessential trace element that is now being commonly utilized in modern technologies, necessitating concerns as to its release in high concentrations to the environment. The sequestration of Co as sulfide nanominerals is promising for environmental remediation and resource recovery and likely played an important role in constraining Co bioavailability in sulfidic oceans on the early Earth. All of these processes will benefit from a better characterization of the initial precipitates and transformation

https://dx.doi.org/10.1021/acs.est.0c01363
Environ. Sci. Technol. XXXX, XXX, XXX−XXX

products of Co-bearing phases under Earth surface aqueous conditions. In this study, we have determined that the initial precipitates were amorphous Co sulfide nanoparticles with a composition of $CoS_{1.00-1.38}{\cdot}xH_2O$ and a log K^* value of 0.9−1.4 at acidic pH (i.e., pH 3.6). This precipitate was stable in anoxic solution at room temperature for 2 months. In the presence of S^0, acidic pH, and temperatures of 60 °C, the Co sulfide nanoparticles undergo transformation to form nanocrystalline jaipurite. Precipitation in the presence of $Fe(II)_{aq}$ and SRB at ambient temperature and near-neutral pH tends to increase the crystallinity of this initial precipitate, yielding nanocrystalline cobalt pentlandite. At equimolar Co and Fe concentrations, the formation of Co-rich mackinawite was highly favored. Our study therefore provides a framework for predicting the primary Co-bearing phase(s) in sulfidic environments. In polluted sites with high $[Co]_{aq}/[Fe]_{aq}$ ratios, the mobility and fate of Co will depend strongly on the solubility and reactivity of discrete Co sulfide nanoparticles such as amorphous Co sulfides, jaipurite, and cobalt pentlandite. Our solubility analysis indicates that the current log K^* values for Co sulfides in popular geochemical databases are inaccurate and can underestimate aqueous Co concentrations by 1−5 orders of magnitude. These misleading values likely have led to falsely positive estimates as to the efficiency of Co precipitation in remediation and resource recovery processes and to lower predictions of bioavailable Co on the sulfidic early Earth. On the other hand, in most pristine environments (i.e., oceans, rivers) or polluted sites with equimolar or low $[Co]_{aq}/[Fe]_{aq}$ ratios, the fate of Co will depend strongly on its interaction with Fe sulfides such as mackinawite and pyrite, with their own associated solubilities and reactivities. Our study has therefore filled a significant knowledge gap in the biogeochemistry of Co in sulfidic environments.

■ ASSOCIATED CONTENT

Supporting Information

Supporting Information includes SI Discussions, Figure S1−S8 and Table S1−S5 provided in a single document. The Supporting Information is available free of charge at https://pubs.acs.org/doi/10.1021/acs.est.0c01363.

Discussions and additional images and data as detailed in the text (PDF)

■ AUTHOR INFORMATION

Corresponding Authors

Muammar Mansor − *Department of Geological Sciences, The University of Texas at El Paso, El Paso, Texas 79968, United States;* orcid.org/0000-0001-7830-650X; Email: mbmansor@utep.edu

Jie Xu − *Department of Geological Sciences, The University of Texas at El Paso, El Paso, Texas 79968, United States;* Email: jxu2@utep.edu

Authors

Elizabeth Cantando − *Virginia Tech National Center for Earth and Environmental Nanotechnology (NanoEarth), Blacksburg, Virginia 24061, United States*

Yi Wang − *Chemistry & Biochemistry Department, The University of Texas at El Paso, El Paso, Texas 79968, United States*

Jose A. Hernandez-Viezcas − *Chemistry & Biochemistry Department and University of California Center for Environmental Implications of Nanotechnology (UC CEIN), The University of Texas at El Paso, El Paso, Texas 79968, United States*

Jorge L. Gardea-Torresdey − *Chemistry & Biochemistry Department and University of California Center for Environmental Implications of Nanotechnology (UC CEIN), The University of Texas at El Paso, El Paso, Texas 79968, United States;* orcid.org/0000-0002-9467-0536

Michael F. Hochella, Jr. − *Virginia Tech National Center for Earth and Environmental Nanotechnology (NanoEarth), Blacksburg, Virginia 24061, United States; Energy and Environment Directorate, Pacific Northwest National Laboratory, Richland, Washington 99354, United States*

Complete contact information is available at: https://pubs.acs.org/10.1021/acs.est.0c01363

Funding

This study was funded by grant DOE-BES DE-FG02-06ER15786 awarded by the United States Department of Energy to M.F.H., J.X., and Mitsu Murayama and also by the start-up package awarded to J.X. by the University of Texas at El Paso. J.L.G.-T. acknowledges the (i) NSF and EPA under Cooperative Agreement Number DBI-1266377, (ii) USDA grant 2016-67021-24985, (iii) NSF Grants EEC-1449500, CHE-0840525, and DBI-1429708, and (iv) the Dudley family for the Endowed Research Professorship and the University of Texas System's STARs Retention Award. Partial funding was provided by the NSF ERC on Nanotechnology-Enabled Water Treatment (EEC-1449500).

Notes

The authors declare no competing financial interest.

■ ACKNOWLEDGMENTS

This work utilized shared facilities at the Virginia Tech National Center for Earth and Environmental Nanotechnology Infrastructure (NanoEarth), a member of the National Nanotechnology Coordinated Infrastructure (NNCI) network, supported by the NSF (ECCS 1542100). NanoEarth is housed at Virginia Tech's Institute for Critical Technology and Applied Sciences (ICTAS). We extend our thanks to Chris Winkler (TEM imaging) and Olivia Fernandez-Delgado (FTIR and TGA) for helping us with the respective analyses.

■ REFERENCES

(1) Romine, M. F.; Rodionova, I. A.; Kim, Y.-M.; Nandhikonda, P.; Clauss, T. R. W.; Anderson, L. N.; Maezato, Y.; Li, X.; Metz, T. O.; Rodionov, D. A.; Xu, C.; Carre, A.; Wright, A. T. Elucidation of Roles for Vitamin B_{12} in Regulation of Folate, Ubiquinone, and Methionine Metabolism. *Proc. Natl. Acad. Sci. U. S. A.* **2017**, *114* (7), E1205−E1214.

(2) Klug, G. Beyond Catalysis: Vitamin B_{12} as a Cofactor in Gene Regulation. *Mol. Microbiol.* **2014**, *91* (4), 635−640.

(3) Rodriguez, I. B.; Ho, T.-Y. Influence of Co and B_{12} on the Growth and Nitrogen Fixation of *Trichodesmium*. *Front. Microbiol.* **2015**, *6*, 1−9.

(4) Roth, J.; Lawrence, J.; Bobik, T. Cobalamin (Coenzyme B_{12}): Synthesis and Biological Significance. *Annu. Rev. Microbiol.* **1996**, *50* (1), 137−181.

(5) Nielsen, M. J.; Rasmussen, M. R.; Andersen, C. B. F.; Nexø, E.; Moestrup, S. K. Vitamin B_{12} Transport from Food to the Body's Cells - A Sophisticated, Multistep Pathway. *Nat. Rev. Gastroenterol. Hepatol.* **2012**, *9* (6), 345−354.

(6) Gál, J.; Hursthouse, A.; Tatner, P.; Stewart, F.; Welton, R. Cobalt and Secondary Poisoning in the Terrestrial Food Chain: Data Review and Research Gaps to Support Risk Assessment. *Environ. Int.* **2008**, *34* (6), 821−838.
(7) Paulo, L. M.; Ramiro-Garcia, J.; van Mourik, S.; Stams, A. J. M.; Sousa, D. Z. Effect of Nickel and Cobalt on Methanogenic Enrichment Cultures and Role of Biogenic Sulfide in Metal Toxicity Attenuation. *Front. Microbiol.* **2017**, *8* (JUL), 1−12.
(8) ATSDR. Toxicological Profile for Cobalt. *U.S Public Heal. Serv. Agency Toxic Subst. Dis. Regist.* **2004**, 121−189.
(9) EPA. Contaminant Candidate List 3 - CCL 3; https://www.epa.gov/ccl/contaminant-candidate-list-3-ccl-3#tech_support_docs (accessed Mar 29, 2019).
(10) NRC. *Groundwater and Soil Cleanup: Improving Management of Persistent Contaminants*; National Academies Press: Washington, D.C., 1999.
(11) Mudd, G. M.; Weng, Z.; Jowitt, S. M.; Turnbull, I. D.; Graedel, T. E. Quantifying the Recoverable Resources of By-Product Metals: The Case of Cobalt. *Ore Geol. Rev.* **2013**, *55* (C), 87−98.
(12) Truex, M. J.; Dresel, P. E.; Nimmons, M. J.; Johnson, C. D. *Screening of Potential Remediation Methods for the 200-BP-5 Operable Unit at the Hanford Site*; Pacific Northwest National Laboratory: Richland, WA, 2006.
(13) Blessing, T. C.; Wielinga, B. W.; Morra, M. J.; Fendorf, S. Co^{III}EDTA- Reduction by *Desulfovibrio Vulgaris* and Propagation of Reactions Involving Dissolved Sulfide and Polysulfides. *Environ. Sci. Technol.* **2001**, *35* (8), 1599−1603.
(14) Krumholz, L. R.; Elias, D. A.; Suflita, J. M. Immobilization of Cobalt by Sulfate-Reducing Bacteria in Subsurface Sediments. *Geomicrobiol. J.* **2003**, *20* (1), 61−72.
(15) Lewis, A. E. Review of Metal Sulphide Precipitation. *Hydrometallurgy* **2010**, *104* (2), 222−234.
(16) Rickard, D.; Luther, G. W. Metal Sulfide Complexes and Clusters. *Rev. Mineral. Geochem.* **2006**, *61* (1), 421−504.
(17) Swanner, E. D.; Planavsky, N. J.; Lalonde, S. V.; Robbins, L. J.; Bekker, A.; Rouxel, O. J.; Saito, M. A.; Kappler, A.; Mojzsis, S. J.; Konhauser, K. O. Cobalt and Marine Redox Evolution. *Earth Planet. Sci. Lett.* **2014**, *390*, 253−263.
(18) Moore, E. K.; Hao, J.; Prabhu, A.; Zhong, H.; Jelen, B. I.; Meyer, M.; Hazen, R. M.; Falkowski, P. G. Geological and Chemical Factors That Impacted the Biological Utilization of Cobalt in the Archean Eon. *J. Geophys. Res.: Biogeosci.* **2018**, *123* (3), 743−759.
(19) Eskelsen, J. R.; Xu, J.; Chiu, M.; Moon, J. W.; Wilkins, B.; Graham, D. E.; Gu, B.; Pierce, E. M. Influence of Structural Defects on Biomineralized ZnS Nanoparticle Dissolution: An in-Situ Electron Microscopy Study. *Environ. Sci. Technol.* **2018**, *52* (3), 1139−1149.
(20) Xu, J.; Murayama, M.; Roco, C. M.; Veeramani, H.; Michel, F. M.; Rimstidt, J. D.; Winkler, C.; Hochella, M. F. Highly-Defective Nanocrystals of ZnS Formed via Dissimilatory Bacterial Sulfate Reduction: A Comparative Study with Their Abiogenic Analogues. *Geochim. Cosmochim. Acta* **2016**, *180*, 1−14.
(21) Bosch, J.; Lee, K. Y.; Jordan, G.; Kim, K. W.; Meckenstock, R. U. Anaerobic, Nitrate-Dependent Oxidation of Pyrite Nanoparticles by *Thiobacillus Denitrificans*. *Environ. Sci. Technol.* **2012**, *46* (4), 2095−2101.
(22) Liu, J.; Aruguete, D. M.; Murayama, M.; Hochella, M. F., Jr Influence of Size and Aggregation on the Reactivity of an Environmentally and Industrially Relevant Nanomaterial (PbS). *Environ. Sci. Technol.* **2009**, *43*, 8178−8183.
(23) Yan, R.; Kappler, A.; Muehe, E. M.; Knorr, K. Effect of Reduced Sulfur Species on Chemolithoautotrophic Pyrite Oxidation with Nitrate. *Geomicrobiol. J.* **2018**, 1−10.
(24) Mansor, M.; Berti, D.; Hochella, M. F., Jr; Murayama, M.; Xu, J. Phase, Morphology, Elemental Composition and Formation Mechanisms of Biogenic and Abiogenic Fe-Cu-Sulfide Nanoparticles: A Comparative Study on Their Occurrences under Anoxic Conditions. *Am. Mineral.* **2019**, *104* (5), 703−717.
(25) Mansor, M.; Winkler, C.; Hochella, M. F., Jr; Xu, J. Nanoparticulate Nickel-Hosting Phases in Sulfidic Environments: Effects of Ferrous Iron and Bacterial Presence on Mineral Formation Mechanism and Solid-Phase Nickel Distribution. *Front. Earth Sci. - Earth Planet. Mater.* **2019**, *7*, 151.
(26) Schoonen, M. A.; Barnes, H. L. Reactions Forming Pyrite and Marcasite from Solution: II. Via FeS Precursors below 100°C. *Geochim. Cosmochim. Acta* **1991**, *55* (6), 1505−1514.
(27) Wilkin, R. T.; Barnes, H. L. Pyrite Formation by Reactions of Iron Monosulfides with Dissolved Inorganic and Organic Sulfur Species. *Geochim. Cosmochim. Acta* **1996**, *60* (21), 4167−4179.
(28) Wilkin, R. T.; Rogers, D. A. Nickel Sulfide Formation at Low Temperature: Initial Precipitates, Solubility and Transformation Products. *Environ. Chem.* **2010**, *7*, 514−523.
(29) Newbury, D. E.; Ritchie, N. W. M. Performing Elemental Microanalysis with High Accuracy and High Precision by Scanning Electron Microscopy/Silicon Drift Detector Energy-Dispersive X-Ray Spectrometry (SEM/SDD-EDS). *J. Mater. Sci.* **2015**, *50* (2), 493−518.
(30) Rickard, D.; Griffith, A.; Oldroyd, A.; Butler, I. B.; Lopez-Capel, E.; Manning, D. A. C.; Apperley, D. C. The Composition of Nanoparticulate Mackinawite, Tetragonal Iron(II) Monosulfide. *Chem. Geol.* **2006**, *235* (3−4), 286−298.
(31) Huang, S.; Lopez-Capel, E.; Manning, D. A. C.; Rickard, D. The Composition of Nanoparticulate Nickel Sulfide. *Chem. Geol.* **2010**, *277* (3−4), 207−213.
(32) Loussot, C.; Pichon, C.; Afanasiev, P.; Vrinat, M.; Pijolat, M.; Valdivieso, F.; Chevarier, A.; Millard-Pinard, N.; Leverd, P. C. Trapping of Radiolytic Hydrogen by Amorphous Cobalt Oxysulfide. *J. Nucl. Mater.* **2006**, *359* (3), 238−246.
(33) Loussot, C.; Afanasiev, P.; Vrinat, M.; Jobic, H.; Leverd, P. C. Amorphous Cobalt Oxysulfide as a Hydrogen Trap. *Chem. Mater.* **2006**, *18* (24), 5659−5668.
(34) Huang, S.; Harris, K. D. M.; Lopez-Capel, E.; Manning, D. A. C.; Rickard, D. Amorphous Nickel Sulfide" Is Hydrated Nanocrystalline NiS with a Core-Shell Structure. *Inorg. Chem.* **2009**, *48* (24), 11486−11488.
(35) Kumar, N.; Raman, N.; Sundaresan, A. Synthesis and Properties of Cobalt Sulfide Phases: CoS2 and Co_9S8. *Z. Anorg. Allg. Chem.* **2014**, *640* (6), 1069−1074.
(36) Aslan, E.; Akin, I.; Patir, I. H. Highly Active Cobalt Sulfide/Carbon Nanotube Catalyst for Hydrogen Evolution at Soft Interfaces. *Chem. - Eur. J.* **2016**, *22* (15), 5342−5349.
(37) Tao, F.; Zhao, Y. Q.; Zhang, G. Q.; Li, H. L. Electrochemical Characterization on Cobalt Sulfide for Electrochemical Supercapacitors. *Electrochem. Commun.* **2007**, *9* (6), 1282−1287.
(38) Kristl, M.; Dojer, B.; Gyergyek, S.; Kristl, J. Synthesis of Nickel and Cobalt Sulfide Nanoparticles Using a Low Cost Sonochemical Method. *Heliyon* **2017**, *3* (3), e00273.
(39) Sun, Y.; Liu, C.; Grauer, D. C.; Yano, J.; Long, J. R.; Yang, P.; Chang, C. J. Electrodeposited Cobalt-Sulfide Catalyst for Electrochemical and Photoelectrochemical Hydrogen Generation from Water. *J. Am. Chem. Soc.* **2013**, *135* (47), 17699−17702.
(40) Kornienko, N.; Resasco, J.; Becknell, N.; Jiang, C. M.; Liu, Y. S.; Nie, K.; Sun, X.; Guo, J.; Leone, S. R.; Yang, P. *Operando* Spectroscopic Analysis of an Amorphous Cobalt Sulfide Hydrogen Evolution Electrocatalyst. *J. Am. Chem. Soc.* **2015**, *137* (23), 7448−7455.
(41) Steefel, C. I.; Appelo, C. A. J.; Arora, B.; Jacques, D.; Kalbacher, T.; Kolditz, O.; Lagneau, V.; Lichtner, P. C.; Mayer, K. U.; Meussen, J. C. L.; Molins, S.; Moulton, D.; Shao, H.; Šimůnek, J.; Spycher, N.; Yabusaki, S. B.; Yeh, G. T. Reactive Transport Codes for Subsurface Environmental Simulation. *Comput. Geosci.* **2015**, *19* (3), 445−478.
(42) Wilkin, R. T.; Beak, D. G. Uptake of Nickel by Synthetic Mackinawite. *Chem. Geol.* **2017**, *462* (April), 15−29.
(43) Hunger, S.; Benning, L. G. Greigite: A True Intermediate on the Polysulfide Pathway to Pyrite. *Geochem. Trans.* **2007**, *8*, 1−20.
(44) Benning, L. G.; Wilkin, R. T.; Barnes, H. L. Reaction Pathways in the Fe-S System below 100°C. *Chem. Geol.* **2000**, *167* (1−2), 25−51.

https://dx.doi.org/10.1021/acs.est.0c01363
Environ. Sci. Technol. XXXX, XXX, XXX−XXX

(45) Matamoros-Veloza, A.; Stawski, T. M.; Benning, L. G. Nanoparticle Assembly Leads to Mackinawite Formation. *Cryst. Growth Des.* **2018**, *18* (11), 6757−6764.
(46) Morse, J. W.; Luther, G. W. Chemical Influence on Trace Metal-Sulfide Interactions in Anoxic Sediments. *Geochim. Cosmochim. Acta* **1999**, *63*, 3373−3378.
(47) Houben, G. J.; Sitnikova, M. A.; Post, V. E. A. Terrestrial Sedimentary Pyrites as a Potential Source of Trace Metal Release to Groundwater - A Case Study from the Emsland, Germany. *Appl. Geochem.* **2017**, *76*, 99−111.
(48) Baidya, A. S.; Sen, A.; Pal, D. C. Textures and Compositions of Cobalt Pentlandite and Cobaltian Mackinawite from the Madan-Kudan Copper Deposit, Khetri Copper Belt, Rajasthan, India. *J. Earth Syst. Sci.* **2018**, *127* (4), 1−15.
(49) Clark, A. H. Nickelian Mackinawite from Vlakfontein, Transfaal: A Discussion. *Mineral. Notes* **1970**, *55* (1969), 1802−1807.
(50) Bortnikova, S.; Bessonova, E.; Gaskova, O. Geochemistry of Arsenic and Metals in Stored Tailings of a Co-Ni Arsenide-Ore, Khovu-Aksy Area, Russia. *Appl. Geochem.* **2012**, *27* (11), 2238−2250.
(51) Eppinger, R. G.; Briggs, P. H.; Rieffenberger, B.; Van Dorn, C.; Brown, Z. A.; Crock, J. G.; Hageman, P. H.; Meier, A.; Sutley, S. J.; Theodorakos, P. M.; Wilson, S. A. Geochemical Data for Stream Sediment and Surface Water Samples from Panther Creek, the Middle Fork of the Salmon River, and the Main Salmon River, Collected before and after the Clear Creek, Little Pistol, and Shellrock Wildfires of 2000 in Central Idaho: 2003; pp 1−32. http://pubs.usgs.gov/of/2003/152/.
(52) Kwong, Y. T. J.; Beauchemin, S.; Hossain, M. F.; Gould, W. D. Transformation and Mobilization of Arsenic in the Historic Cobalt Mining Camp, Ontario, Canada. *J. Geochem. Explor.* **2007**, *92* (2−3), 133−150.
(53) Thoenen, T. Pitfalls in the Use of Solubility Limits for Radioactive Waste Disposal: The Case of Nickel Sulfidic Groundwaters. *Nucl. Technol.* **1999**, *126* (1), 75−87.
(54) Lee, G.; Bigham, J. M.; Faure, G. Removal of Trace Metals by Coprecipitation with Fe, Al and Mn from Natural Waters Contaminated with Acid Mine Drainage in the Ducktown Mining District, Tennessee. *Appl. Geochem.* **2002**, *17* (5), 569−581.
(55) Heikkinen, P. M.; Korkka-Niemi, K.; Lahti, M.; Salonen, V. P. Groundwater and Surface Water Contamination in the Area of the Hitura Nickel Mine, Western Finland. *Environ. Geol.* **2002**, *42* (4), 313−329.
(56) Rahman, M. M.; Dong, Z.; Naidu, R. Concentrations of Arsenic and Other Elements in Groundwater of Bangladesh and West Bengal, India: Potential Cancer Risk. *Chemosphere* **2015**, *139*, 54−64.
(57) Bruland, K. W.; Middag, R.; Lohan, M. C. Controls of Trace Metals in Seawater. In *Treatise on Geochemistry*, 2nd ed.; Elsevier: 2013; Vol. *8*, pp 19−51. DOI: 10.1016/B978-0-08-095975-7.00602-1.
(58) Gaillardet, J.; Viers, J.; Dupré, B. Trace Elements in River Waters. In *Treatise on Geochemistry*, 2nd ed.; Turekian, K., Holland, H., Eds.; Elsevier: 2013; pp 195−235. DOI: 10.1016/B978-0-08-095975-7.00507-6.
(59) Picard, A.; Gartman, A.; Girguis, P. R. What Do We Really Know about the Role of Microorganisms in Iron Sulfide Mineral Formation? *Front. Earth Sci.* **2016**, *4*, 1−10.
(60) Picard, A.; Gartman, A.; Clarke, D. R.; Girguis, P. R. Sulfate-Reducing Bacteria Influence the Nucleation and Growth of Mackinawite and Greigite. *Geochim. Cosmochim. Acta* **2018**, *220*, 367−384.
(61) Gramp, J. P.; Sasaki, K.; Bigham, J. M.; Karnachuk, O. V.; Tuovinen, O. H. Formation of Covellite (CuS) under Biological Sulfate-Reducing Conditions. *Geomicrobiol. J.* **2006**, *23* (8), 613−619.
(62) Gramp, J. P.; Bigham, J. M.; Jones, F. S.; Tuovinen, O. H. Formation of Fe-Sulfides in Cultures of Sulfate-Reducing Bacteria. *J. Hazard. Mater.* **2010**, *175* (1−3), 1062−1067.
(63) Moreau, J. W.; Weber, P. K.; Martin, M. C.; Gilbert, B.; Hutcheon, I. D.; Banfield, J. F. Extracellular Proteins Limit the Dispersal of Biogenic Nanoparticles. *Science (Washington, DC, U. S.)* **2007**, *316*, 1600−1603.
(64) Fein, J. B.; Martin, A. M.; Wightman, P. G. Metal Adsorption onto Baterial Surfaces: Development of a Predictive Approach. *Geochim. Cosmochim. Acta* **2001**, *65* (23), 4267−4273.
(65) Beveridge, T. J.; Koval, S. F. Binding of Metals to Cell Envelopes of *Escherichia Coli* K-12. *Appl. Environ. Microbiol.* **1981**, *42* (2), 325−335.
(66) Beveridge, T. J.; Murray, R. G. E. Uptake and Retention of Metals by Cell Walls of *Bacillus Subtilis*. *J. Bacteriol.* **1976**, *127* (3), 1502−1518.
(67) Ferris, F.; Schultze, S.; Witten, T.; Fyfe, W.; Beveridge, T.; Schultz, S. Metal Interactions with Microbial Biofilms in Acidic and Neutral PH Environments. *Appl. Environ. Microbiol.* **1989**, *55* (5), 1249−1257.
(68) Ikuma, K.; Decho, A. W.; Lau, B. L. T. When Nanoparticles Meet Biofilms - Interactions Guiding the Environmental Fate and Accumulation of Nanoparticles. *Front. Microbiol.* **2015**, *6*, 1−6.
(69) Bourdoiseau, J. A.; Jeannin, M.; Rémazeilles, C.; Sabot, R.; Refait, P. The Transformation of Mackinawite into Greigite Studied by Raman Spectroscopy. *J. Raman Spectrosc.* **2011**, *42* (3), 496−504.
(70) White, L. M.; Bhartia, R.; Stucky, G. D.; Kanik, I.; Russell, M. J. Mackinawite and Greigite in Ancient Alkaline Hydrothermal Chimneys: Identifying Potential Key Catalysts for Emergent Life. *Earth Planet. Sci. Lett.* **2015**, *430*, 105−114.
(71) Moreno Flores, E. A. *Precipitation and Transformation of Iron-Sulfide Nanoparticles in Low-Temperature Aqueous Environment: Effects of Reactant Iron and Sulfide Sources*; University of Texas at El Paso, 2019.
(72) Pejova, B.; Isahi, A.; Najdoski, M.; Grozdanov, I. Fabrication and Characterization of Nanocrystalline Cobalt Oxide Thin Films. *Mater. Res. Bull.* **2001**, *36* (1−2), 161−170.

https://dx.doi.org/10.1021/acs.est.0c01363
Environ. Sci. Technol. XXXX, XXX, XXX−XXX